

# The cosmic rays mediated nonpolytropic solar wind interacting with the interstellar neutral matter

M. Banaszkiewicz and J. Ziemkiewicz

Space Research Center, Bartycka 18a, PL-00716 Warsaw, Poland

Received 14 January 1997 / Accepted 29 May 1997

**Abstract.** The solar wind spherical flow is considered under the combined action of gas pressure, magnetic field pressure and pressures of cosmic rays; both galactic and anomalous component. The interaction of solar wind ions with LISM neutrals is taken into account self-consistently by introducing the appropriate source terms in the flow equations. The numerical solutions of a set of five differential equations describing the system, obtained for different model parameters, provide a spectrum of possible configurations of the outer heliosphere. The formation of the solar wind termination shock is described and the shock position and strength are studied. The nonpolytropic solar wind is considered; the difference between the calculated pressure and the one resulting from the polytropic law are discussed. While taking into account the effects connected with the production of superthermal population leads to an increase of the shock compression ratio, the interaction with the LISM neutrals results in weaker shocks. The galactic cosmic rays push the shock inward, the anomalous component cosmic rays move it outward. Several sets of input parameters such as the initial speed and density of the solar wind (fast or slow), the cosmic ray diffusion coefficients, the density of interstellar neutrals, and the efficiency of the cosmic ray production at the shock are considered. For a typical distance to the solar wind termination shock of 60-100 AU, the efficiency of the cosmic rays production must be in the range 0-15%, in order to obtain well-behaved solutions in the downwind region.

**Key words:** heliosphere – solar wind – termination shock – cosmic rays – pickup ions

---

## 1. Introduction

The solar wind flows out from the Sun with the approximate spherical symmetry and meets on its way the local interstellar matter (LISM). Since the wind is supersonic, the presence of the LISM cannot be communicated to the wind via hydromagnetic

mechanisms, and deceleration of the flow is realized in the form of a shock wave. The position of this shock has been the subject of intensive studies during the last decade (Fahr et al. 1988, Fahr & Fichtner 1991, Grzedzielski & Ziemkiewicz; 1989, 1990, Donohue & Zank 1993, Ziemkiewicz & Banaszkiewicz 1996) and the expected radial distance was shown to lie somewhere between 50 and 150 AU. This discrepancy in the results shows that the knowledge of the LISM parameters and of the physical processes important in the outer heliosphere is still insufficient to give a clear answer to this question. The recent modelling studies (Zank et al. 1996a, 1996b, Pauls & Zank, 1996) as well as the results of space missions indicate that the range of shock radii is limited to 70-110 AU in the equatorial plane. As Voyager and Pioneer probes are now approaching the region where the shock may be found, the problem becomes very important.

The interstellar plasma interacts strongly with the plasma of the wind at the edges of the heliosphere. The neutral components of the LISM penetrate the heliosphere. Some of them (e.g. helium) have almost free access. Others, like hydrogen, react easily with the dense compressed plasma in the heliosheath. As the result their number density may be reduced by 50% and their bulk velocity may decrease from 26 to 20 km/s (Zank et al. 1996b). Since the LISM bulk velocity is much smaller than the solar wind velocity, such a freshly born ion may be considered to be at rest with respect to the Sun. These ions are immediately picked up by the solar wind electromagnetic fields to become the so called pickup ion population; the acceleration of these particles from  $v=0$  to  $v=400$  km/s results in the losses of the solar wind momentum and energy fluxes. The pickup ions and their effect on the solar wind flow have been studied theoretically in several papers (Fahr & Fichtner 1991, Isenberg 1995, Isenberg & Lee 1995, Zank et al. 1996a,b, Williams et al. 1995, Lee 1995). A small but important fraction of the pickup ions is injected at the shock into the process of the diffusive acceleration and becomes the anomalous cosmic rays (see below). In the present model the photoionisation of LISM neutrals and the charge-exchange between them and solar wind ions are taken into account in the form of source terms appearing in the hydrodynamic equations.

---

*Send offprint requests to:* M. Banaszkiewicz

Thanks to their large diffusion coefficient, the galactic cosmic rays (GCR) can penetrate the heliosphere, where, because of the solar wind convection, their spectrum becomes modulated i.e. dependent on the distance to the Sun (McKibben et al., 1996). Several models of the cosmic ray modified solar wind have been constructed up to now (Webb & McKenzie 1984, Ko & Webb 1987, 1988, Ko et al 1988, 1991, Ko 1991), among which the earliest study the cosmic rays in the test particle approximation, i.e. consider the undisturbed background flow, and the latest include all the nonlinear effects that arise in the system i.e. take into account not only the fact that the gradient force of the cosmic rays slows down the solar wind flow, which in turn changes the cosmic ray pressure etc., but also the interaction with the cosmic ray induced turbulence.

Acceleration of charged particles to superthermal energies should always be taken into account if the formation of a collisionless shock wave is considered. It is now commonly believed that the population less energetic (10-100 MeV/nucl.) than GCR, called the anomalous component cosmic rays (ACR), is produced at the solar wind termination shock (McKibben et al., 1996). This constituent, which diffuses in both directions outwards from the shock, can modify the background flow and take part in the nonlinear interaction. Diffusive acceleration of a small fraction of pickup ions with energy initially 1 keV/nucl. to energy 10 MeV/nucl. is an energetically expensive process; while the losses in the solar wind mass flux can be neglected, the sink in the energy flux is not negligible and should be taken into account. A number of papers (Donohue & Zank 1993, Fichtner et al. 1993, Zank et al. 1993, Barnes 1994, Chalov & Fahr 1994, 1995, Ziemkiewicz 1994, 1995) dealt recently with this problem. The models describing the influence of cosmic rays and of interstellar gas on polytropic wind dynamics have been recently reviewed by Lee (1995).

The present paper is the first one in which the cosmic ray modified nonpolytropic solar wind interacting with the neutral interstellar gas is considered. The model relies on considering the three fluid medium : the background plasma and the massless, galactic as well as anomalous component cosmic rays. We are interested in the stationary, spherically symmetric, magnetized, non-polytropic background plasma. Because of numerous kinematical and dynamical effects present in the inner solar wind (such as changes of the wind parameters and interplanetary shock waves (Burton et al., 1996)), the shock is in a constant in and out motion (Barnes 1993, Story & Zank, 1995), therefore our stationary model can describe an average outer heliosphere configuration only (Donohue & Zank 1993, Ziemkiewicz 1994). The process of the solar wind interaction with interstellar neutrals, which leads to the formation of the pickup ion population, is taken into account in a self-consistent approach by introducing the appropriate source terms into the hydrodynamic equations. The model and the numerical algorithm are briefly outlined in the next section.

Since the recent results of the Ulysses mission (Goldstein et al., 1996, Feldman et al., 1996) show a qualitative and quantitative difference between the equatorial and high-latitude solar wind flows, we solve our problem for two sets of input param-

eters typical for either slow equatorial or fast polar winds. Also two sets of neutral gas parameters resulting in high and low reaction rates with the solar wind are considered. In Sect. 3 we present the results as they depend on three parameters that control the solutions: cosmic ray diffusion coefficients, position (distance) of the termination shock, and the efficiency of the cosmic ray production at the shock. In the last section we discuss the relevance of the obtained results and come to our conclusions.

## 2. Model equations

The dynamics of the system is constrained by the overall mass, momentum and energy equations of the background plasma supplemented by the second moment of the cosmic ray transport equations (called the diffusion equations hereafter). The three steady-state hydrodynamic equations for the gas density  $\rho$ , velocity  $v$  and pressure  $P$  take the form:

$$\nabla \cdot (\rho \mathbf{v}) = q_{\text{mass}} \quad (1)$$

$$\rho(\mathbf{v} \cdot \nabla) \mathbf{v} = -\nabla P - \nabla P^G - \nabla P^A + \mathbf{f}^M + \mathbf{q}_{\text{mom}} \quad (2)$$

$$\nabla \cdot (\mathbf{F}^G + \mathbf{F}^M + \mathbf{F}^A) = q_{\text{en}} \quad (3)$$

where  $P^G$ ,  $P^A$ ,  $\mathbf{F}^G$ ,  $\mathbf{F}^A$  are the GCR and ACR pressures and energy fluxes,  $\mathbf{F}^G$  and  $\mathbf{F}^M$  are the gas and magnetized energy fluxes, and the Lorenz force is:

$$\mathbf{f}^M = -\frac{1}{4\pi} \mathbf{B} \times (\nabla \times \mathbf{B}) \quad (4)$$

The model takes into account the plasma interaction with the neutral interstellar matter i.e. the photoionisation of the neutral H and He and the charge exchange between the thermal ions and atomic hydrogen. While the process of charge exchange with hydrogen does not affect the flux of mass, the photoionisation introduces a source term in the continuity equation. According to the recent paper by Lee (1995), the source terms arising from this interaction upstream of the shock are:

$$q_{\text{mass}} = m_p \left( \frac{r_E}{r} \right)^2 (\nu_H^0 n_{H\infty} + \nu_{He}^0 n_{He\infty}) \quad (5)$$

$$\mathbf{q}_{\text{mom}} = -\sigma n_{H\infty} \rho v^2 \frac{\mathbf{r}}{r} \quad (6)$$

$$q_{\text{en}} = -\sigma n_{H\infty} \frac{1}{2} \rho v^3 \quad (7)$$

where  $m_p$  is the proton mass,  $r_E = 1$  AU,  $\sigma = 2 \times 10^{-15} \text{ cm}^{-2}$  is the charge-exchange cross-section between neutral hydrogen atoms and protons.

In the downwind region, where the flow density increases, photoionization can be neglected and charge-exchange becomes the only important ionization mechanism. It does not contribute to the mass source but, obviously, removes momentum and energy from the flow. Following Holzer (1972) and Lee (1995) we have:

$$q_{\text{mass}} = 0 \quad (8)$$

$$\mathbf{q}_{\text{mom}} = -\sigma n_{\text{H}\infty} \alpha \sqrt{\frac{P}{\rho}} \rho \mathbf{v} \quad (9)$$

$$q_{\text{en}} = -\sigma n_{\text{H}\infty} \alpha \sqrt{\frac{P}{\rho}} \frac{P}{\gamma - 1} \quad (10)$$

with  $\alpha = \sqrt{128/9\pi}$ . The source terms (5)-(7) and (8)-(10) are approximate (see Pauls et al. 1995 for the exact forms). The approximation is quite good in the upwind region, but overestimates the momentum and energy transfer to the subsonic solar wind flow in the heliosheath.

We have included the magnetic field into the model. In the presence of the magnetic field the position of the termination shock for a given interstellar field pressure may be closer to the Sun, as described by the Axford-Cranfill effect (Nerney et al., 1991). However, it has been shown recently (Ziemkiewicz 1994, 1995) that the magnetic field has a weak influence on the termination shock position and on the shock structure. On the other hand, in the outer heliosphere near the equatorial plane, as  $B \propto r$ , the magnetic effects become important in the far downwind region, where the velocity value decreases (Nerney et al. 1993).

The cosmic rays are treated as a massless fluid, representing pressure and energy flux (Axford et al. 1982, Webb & McKenzie 1984). The galactic cosmic rays, present everywhere in space, are scattered by turbulent fields travelling in the background flow and diffuse with the diffusion coefficient  $K$ . The pressure of the galactic cosmic rays is described by:

$$\nabla \cdot \mathbf{F}^{\text{G}} = \mathbf{v} \cdot \nabla P^{\text{G}} \quad (11)$$

The acceleration of charged particles is a mechanism that plays a crucial role in collisionless shock physics (Jones & Ellison, 1993) and it is assumed here that at the solar wind termination shock the anomalous component cosmic rays (ACR) are produced. This population, produced by the shock itself, carries away some part of the background gas energy flux. The ACR diffusion equation has thus the following form:

$$\nabla \cdot \mathbf{F}^{\text{A}} = \mathbf{v} \cdot \nabla P^{\text{A}} + Q \quad (12)$$

where the source term  $Q$  (Webb et al. 1985), that vanishes everywhere except the shock, describes the injection of the gas energy flux into the ACR energy flux. The energy fluxes of the gas and cosmic rays are defined by:

$$\begin{aligned} \mathbf{F}^{\text{g}} &= \rho \mathbf{v} \left( \frac{1}{2} v^2 + \frac{\gamma}{\gamma - 1} \frac{P}{\rho} \right) \\ \mathbf{F}^{\text{G,A}} &= \left( \frac{\gamma}{\gamma - 1} P \mathbf{v} - \frac{1}{\gamma - 1} K \nabla P \right)^{\text{G,A}} \end{aligned} \quad (13)$$

The specific heats ratio  $\gamma = 5/3$  is assumed for the background gas; for the cosmic rays we take  $\gamma_{\text{G}} = 4/3$  and  $\gamma_{\text{A}} = 5/3$ .

In the above equations the terms describing the magnetic effects can be written (in the spherically symmetric case) as:

$$\mathbf{f}^{\text{M}} = -\nabla P^{\text{M}} - \frac{2}{r} P^{\text{M}}, \quad P^{\text{M}} = \frac{1}{8\pi} B^2, \quad F^{\text{M}} = 2P^{\text{M}} v \quad (14)$$

for  $\mathbf{B} \perp \mathbf{v}$ , or:

$$\mathbf{f}^{\text{M}} = 0, \quad P^{\text{M}} = 0, \quad F^{\text{M}} = 0 \quad (15)$$

for  $\mathbf{B} \parallel \mathbf{v}$ . Equation (14) describes the magnetic variables in the ecliptic plane, and (15) in the polar heliosphere.

The conservation laws at the shock (here and in what follows the subscripts 1,2 denote upwind and downwind quantities, respectively and the brackets  $[\cdot]$  denote the jump at the shock) are:

$$[\rho \mathbf{v}]_2^1 = 0 \quad (16)$$

$$[\rho v^2 + P + P^{\text{M}} + P^{\text{G}} + P^{\text{A}}]_2^1 = 0 \quad (17)$$

$$[P^{\text{G}}]_2^1 = 0 \quad (18)$$

$$[P^{\text{A}}]_2^1 = 0 \quad (19)$$

$$[F^{\text{g}} + F^{\text{M}}]_2^1 = \varepsilon \frac{1}{2} \rho_1 v_1^3 \quad (20)$$

$$[F^{\text{A}}]_2^1 = -\varepsilon \frac{1}{2} \rho_1 v_1^3 \quad (21)$$

$$[F^{\text{G}}]_2^1 = 0 \quad (22)$$

where it is assumed that a part  $\varepsilon$  of the solar wind energy flux is spent at the shock to produce the ACR, i.e. the term  $\varepsilon \frac{1}{2} \rho_1 v_1^3$  represents the source term  $Q$  in Eq.(12). Since more energetic GCRs do not feel the solar wind shock, both their pressure and energy flux are continuous across the shock.

Defining the shock compression ratio as

$$q = \frac{v_1}{v_2} = \frac{\rho_2}{\rho_1} \quad (23)$$

the conservation laws at the shock yield the following cubic equation for  $q$ :

$$\begin{aligned} q^3(2 - \gamma) + q^2\{2(\gamma - 1) + \gamma\beta + \frac{1}{2}(1 - \varepsilon)(\gamma\beta + 2)\} \\ \times (\gamma - 1)M^2\} - q\gamma\{1 + \beta + M^2(\gamma\beta + 2)\} \\ + \frac{1}{2}M^2(\gamma + 1)(\gamma\beta + 2) = 0 \end{aligned} \quad (24)$$

where:  $\beta = P/P^{\text{M}}$ , the upwind Mach number  $M = v/\sqrt{c^2 + v_{\text{A}}^2}$ , and  $c, v_{\text{A}}$  are the sound and the Alfvén speeds.

In the spherically symmetric heliosphere, the set of three hydrodynamic equations (1)-(3) and two diffusion equations (11) and (12) constitute a seventh-order system for  $\rho, v, P, P^{\text{G}}, \frac{dP^{\text{G}}}{dr}, P^{\text{A}}$ , and  $\frac{dP^{\text{A}}}{dr}$ . Following Ziemkiewicz (1994) we introduce dimensionless variables:

$$s \equiv \frac{r}{r_{\text{E}}}, \quad x \equiv \frac{\rho}{\rho_{\text{E}}}, \quad y \equiv \frac{v}{v_{\text{E}}},$$

$$z \equiv \frac{P}{\rho_{\text{E}} v_{\text{E}}^2}, \quad z^{\text{G,A,M}} \equiv \frac{P^{\text{G,A,M}}}{\rho_{\text{E}} v_{\text{E}}^2},$$

$$k^{\text{G,A}} = \frac{K^{\text{G,A}}}{\rho_{\text{E}} v_{\text{E}}},$$

$$Q_{\text{mass}} = q_{\text{mass}} \frac{r_E}{\rho_E v_E}, \quad Q_{\text{mom}} = q_{\text{mom}} \frac{r_E}{\rho_E v_E^2},$$

$$Q_{\text{en}} = q_{\text{en}} \frac{r_E}{\rho_E v_E^3}. \quad (25)$$

With the help of formulae (25), Eqs. (1)-(3) and (11)-(12) take the form:

$$\frac{dx}{ds} = \frac{xy \left[ \left( Q_{\text{mass}} - \frac{Q_{\text{mom}}}{y} \right) - \frac{2xy}{s} + \frac{4z^M}{sy} \right]}{(xy^2 - 2z^M)} + \frac{x \left( \frac{dz}{ds} + \frac{dz^G}{ds} + \frac{dz^A}{ds} \right)}{(xy^2 - 2z^M)} \quad (26)$$

$$\frac{dy}{ds} = - \frac{y \left[ Q_{\text{mass}} \frac{2z^M}{xy} - Q_{\text{mom}} + \frac{dz}{ds} + \frac{dz^G}{ds} + \frac{dz^A}{ds} \right]}{(xy^2 - 2z^M)} \quad (27)$$

$$\frac{dz}{ds} = \frac{\frac{2z}{s} \gamma (xy^2 - 2z^M) - \frac{Q_{\text{en}}}{y} (\gamma - 1) (xy^2 - 2z^M)}{(2z^M + \gamma z - xy^2)} + \frac{Q_{\text{mom}} (\gamma - 1) (xy^2 - 2z^M + \frac{\gamma}{\gamma-1} z)}{(2z^M + \gamma z - xy^2)} + \frac{\frac{Q_{\text{mass}}}{y} \left[ (\gamma - 1) \left( \frac{y^2}{2} + \frac{2z^M}{x} \right) (xy^2 - 2z^M) \right]}{(2z^M + \gamma z - xy^2)} - \frac{2Q_{\text{mass}} \gamma \frac{zz^M}{xy} + \gamma z \left( \frac{dz^G}{ds} + \frac{dz^A}{ds} \right)}{(2z^M + \gamma z - xy^2)} \quad (28)$$

$$\frac{d^2 z^G}{ds^2} = - \frac{1}{k^G} \frac{dz^G}{ds} \left( \frac{2}{s} k^G + \frac{dk^G}{ds} - y \right) + \frac{\gamma^G}{k^G} z^G \left( \frac{2y}{s} + \frac{dy}{ds} \right) \quad (29)$$

$$\frac{d^2 z^A}{ds^2} = - \frac{1}{k^A} \frac{dz^A}{ds} \left( \frac{2}{s} k^A + \frac{dk^A}{ds} - y \right) + \frac{\gamma^A}{k^A} z^A \left( \frac{2y}{s} + \frac{dy}{ds} \right) \quad (30)$$

The above equations must be complemented with initial or boundary conditions. In earlier papers attacking a simplified version of the problem (without source terms and for a polytropic gas), an iterative method of solving the boundary value problem has been employed (Ko et al., 1988). In this paper we use a different method, in which Eqs. (26)-(30) are considered as an initial value problem with the values of all unknowns set at 1 AU. In the upwind region we follow the solutions until the assumed position of the shock is reached. The conservation equations together with a prescribed value of  $\varepsilon$  yield the initial values in the downwind region, which are then used to integrate the equations to the heliopause. In this way, we obtain a two-parameter  $(r_{\text{sh}}, \varepsilon)$  family of solutions. Any solution that: (i) gives the right value of  $P^G \sim 0.33 \text{ eV cm}^{-3}$  "at infinity", (ii) yields an appropriate pressure value at the heliopause ( $= P_{\text{LISM}} \sim 1 \text{ eV cm}^{-3}$ ), and (iii) shows the right (i.e. decreasing and non-negative, see Fig. 1) profile of the anomalous cosmic rays pressure in the downwind region is accepted. There is

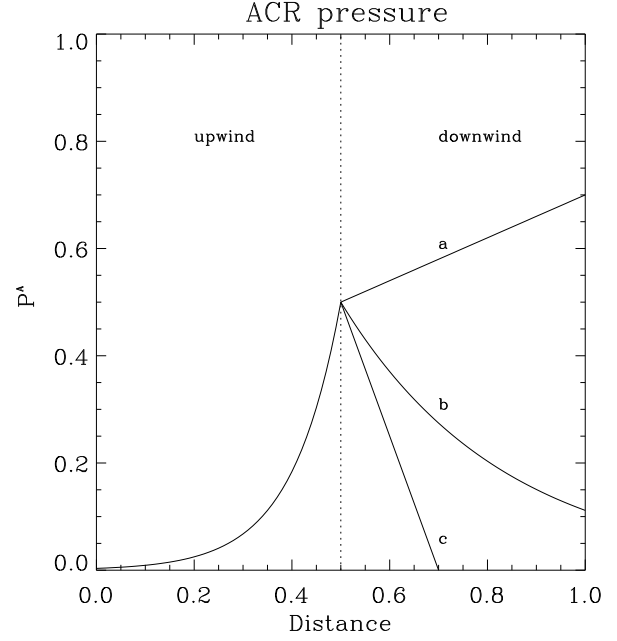


**Fig. 1.** Three types of the ACR pressure profile: (a) corresponds to a source not at the shock, but far in the downwind region (small  $\varepsilon$ ), (c) yields negative values downstream of the shock and is, therefore, unphysical (large  $\varepsilon$ ), (b) is the appropriate one (medium  $\varepsilon$ ). The dotted line denotes the shock position. The units on both axes are arbitrary.

another reason to solve our system of differential equations as an initial value problem. In some cases the solutions may pass through a critical point or a number of critical points. We have not followed the full critical point analysis that would provide one with the topological nature of the solutions, as it was done for a simpler case by Zank (1989). In our numerical approach Eqs. (26)-(30) either become singular for some models, when one of denominators approaches zero, or provide meaningless solutions starting from the point where a numerator has a (double) root. If it happens in the velocity equation, for example, this variable first decreases and then, after passing through its minimum value, starts to increase. Soon, all of the integrated functions are affected. Such cases can be easily identified and diagnosed in the initial value formulation, but would be more difficult to handle by any of the BVP (boundary value problem) solvers.

### 3. Results

We consider several models defined by combinations of input parameters controlling the solutions of Eqs. (26)-(30). They belong to three different groups. First of all, one can choose between the equatorial and the polar solar wind. In the former case the initial values of hydrodynamic parameters at 1 AU are (Schwenn, 1990):

$$n_0 = \frac{\rho_0}{m_p} = 8 \text{ cm}^{-3}, \quad v_0 = 400 \text{ km/s},$$

$$P_0 = 4.4 \times 10^{-11} \text{ erg cm}^{-3} \quad (31)$$

**Table 1.** Models: input parameters and main results

Model	Solar Wind <sup>b</sup>	Neutral Source Rate <sup>d</sup>	$K_1^{G,A}$ [cm <sup>2</sup> /s] <sup>a</sup>	$r_{sh} = 65$ AU			$r_{sh} = 80$ AU			$r_{sh} = 95$ AU		
				$P_\infty^G$	$q$	$\varepsilon$	$P_\infty^G$	$q$	$\varepsilon$	$P_\infty^G$	$q$	$\varepsilon$
1	slow	large	$K^G = 6 \cdot 10^{22} + 1 \cdot 10^{20}r$ $K^A = 6 \cdot 10^{21} + 1 \cdot 10^{19}r$	0.27	3.44	< 0.01	0.31	3.32	0.01	0.34	3.35	0.09
2	slow	large	$K^G = 4 \cdot 10^{22} + 5 \cdot 10^{20}r$ $K^A = 4 \cdot 10^{21} + 5 \cdot 10^{19}r$	0.30	3.43	< 0.01	0.33	3.55	0.07	0.36	3.95	0.15
3	slow	small	$K^G = 6 \cdot 10^{22} + 1 \cdot 10^{20}r$ $K^A = 6 \cdot 10^{21} + 1 \cdot 10^{19}r$	0.28	3.65	< 0.01	0.32	3.59	0.01	0.36	3.50	0.05
4	slow	small	$K^G = 4 \cdot 10^{22} + 5 \cdot 10^{20}r$ $K^A = 4 \cdot 10^{21} + 5 \cdot 10^{19}r$	0.31	3.64	< 0.01	0.35	3.70	0.04	0.37	3.65	0.15
				$r_{sh} = 80$ AU			$r_{sh} = 100$ AU			$r_{sh} = 120$ AU		
				$P_\infty^G$	$q$	$\varepsilon$	$P_\infty^G$	$q$	$\varepsilon$	$P_\infty^G$	$q$	$\varepsilon$
11	fast	large	$K^G = 1 \cdot 10^{23}$ $K^A = 1.5 \cdot 10^{22}$	0.35	3.45	< 0.01	0.43	3.28	0.01	0.51	3.22	0.09
12	fast	large	$K^G = 1 \cdot 10^{23}$ $K^A = 1.18 \cdot 10^{22}$	0.35	3.43	< 0.01	0.42	3.35	0.07	0.48	1.88	0.15
13	fast	small	$K^G = 1 \cdot 10^{23}$ $K^A = 1.5 \cdot 10^{22}$	0.38	3.66	< 0.01	0.48	3.56	0.01	0.57	3.53	0.10
14	fast	small	$K^G = 1 \cdot 10^{23}$ $K^A = 1.22 \cdot 10^{22}$	0.38	3.65	< 0.01	0.46	3.44	0.02	0.53	1.82	0.15

<sup>a</sup> upwind values,  $r$  in AU

<sup>b</sup> Slow and fast solar wind parameters are given by formulae (31) and (32), respectively

<sup>c</sup> in eV/cm<sup>3</sup>

<sup>d</sup> Large and small neutral source rates are obtained from (35) and (34), respectively

while those of the polar wind are (McComas et al., 1995):

$$n_0 = \frac{\rho_0}{m_p} = 3.5 \text{ cm}^{-3}, \quad v_0 = 750 \text{ km/s},$$

$$P_0 = 2.2 \times 10^{-10} \text{ erg cm}^{-3} \quad (32)$$

The pressures above correspond to temperatures of  $4 \times 10^4$  K and  $2 \times 10^5$  K, respectively. The pressures of the cosmic rays components are the same in both models:

$$P_0^G = 1.8 \times 10^{-13} \text{ erg cm}^{-3}$$

$$\frac{dP_0^G}{dr} = 1.8 \times 10^{-14} \text{ erg cm}^{-3} \text{ AU}^{-1}$$

$$P_0^A = 1.8 \times 10^{-17} \text{ erg cm}^{-3}$$

$$\frac{dP_0^A}{dr} = 1.8 \times 10^{-18} \text{ erg cm}^{-3} \text{ AU}^{-1} \quad (33)$$

The pressure of galactic cosmic rays is close to the value of  $0.17 \text{ eV cm}^{-3}$ , typical for the inner heliosphere (Jokipii, 1990). The next set of parameters determines the pick-up ion source terms (Eqs. (5)-(7)). At the solar minimum the densities of neutral components of LISM and their ionization rates at 1 AU are (Lee, 1995):

$$\nu_H^0 = 9 \times 10^{-8} \text{ s}^{-1} \quad n_{H\infty} = 6 \times 10^{-2} \text{ cm}^{-3}$$

$$\nu_{He}^0 = 8 \times 10^{-8} \text{ s}^{-1} \quad n_{He\infty} = 6 \times 10^{-3} \text{ cm}^{-3} \quad (34)$$

The above values correspond to the lower limit of the referenced values. The recent Ulysses data (Witte et al. 1993) suggest that

the density values may even be more than 2 times larger. Also at solar maximum the ionisation rate can significantly increase. Therefore, we will use also the following values:

$$\nu_H^0 = 1.5 \times 10^{-7} \text{ s}^{-1} \quad n_{H\infty} = 1.2 \times 10^{-1} \text{ cm}^{-3}$$

$$\nu_{He}^0 = 1.4 \times 10^{-7} \text{ s}^{-1} \quad n_{He\infty} = 1.5 \times 10^{-2} \text{ cm}^{-3} \quad (35)$$

The last group of parameters consists of the diffusion coefficients for the galactic and anomalous cosmic rays,  $K^G$ ,  $K^A$ . Unfortunately, it is not possible within the framework of the present model to calculate self-consistently the diffusive coupling between the ambient medium (plasma and magnetic field) and the cosmic rays. Moreover, since the diffusion coefficients averaged over the spectrum of energies of each kind of cosmic rays are not well known,  $K^{G,A}$  must in fact be treated as free parameters of the model. It is well known that the diffusion coefficient is a function of the turbulence level  $\delta B/8\pi$  and of the magnetic field  $B$  itself; the diffusion in the direction perpendicular to the field is generally less efficient than the diffusion along the field ( $K_\perp \ll K_\parallel$ ). As the upwind field decreases with  $r$ , we assume that the upwind diffusion coefficients increase:

$$K_1^{G,A} = K_{10}^{G,A} + K_{11}^{G,A} r \quad (36)$$

In the ecliptic plane, where the field is azimuthal, the cross-field diffusion is appropriate; in the polar heliosphere the parallel diffusion coefficient should be taken into account. In the post-shock region both the magnetic field ( $B_2 = qB_1$ ) and the turbulence level increase, but, as the functional dependence of

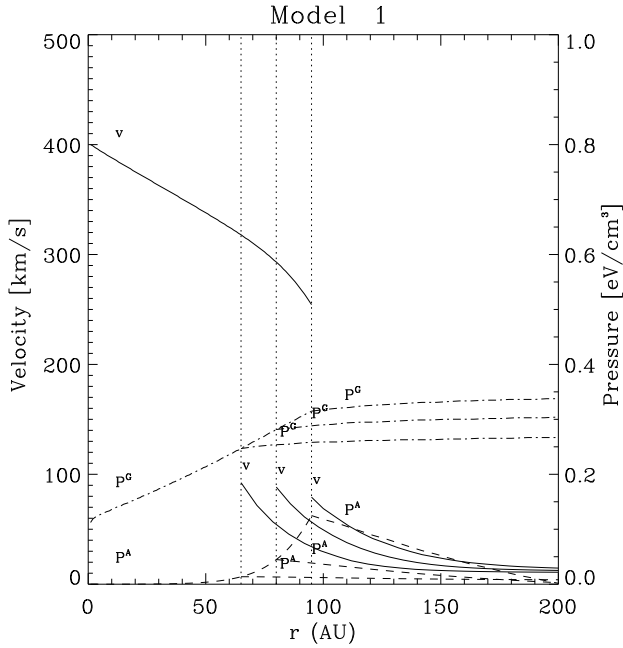


**Fig. 2.** Velocity  $v$  and cosmic rays pressures  $P^G$  and  $P^A$  as functions of a distance for model 1. Three different positions of the shock are indicated by dotted lines; from each one of them the downstream intergration starts and results in a different profile of the considered quantities. The production efficiency  $\varepsilon$  is chosen for each shock as a maximum possible value from the range (0,0.15) still yielding a non-negative ACR pressure downstream of the shock. It is equal 0.0, 0.01, and 0.06 for the shock at 65, 80, and 95 AU, respectively.

$K$  on the field and on the number of scattering centers is not fully known, the value of the downwind diffusion coefficient is difficult to specify. In order not to multiply the amount of numerical results, in this paper we assume that the downwind diffusion coefficients,  $K_2$ , are constant and equal to the upwind values at the shock. According to Potgieter et al. (1987), the diffusion coefficient is proportional to the thermal velocity of diffusing particles, so that  $K^A$ , corresponding to particles with energy 10 MeV, is assumed to be 10 times smaller than  $K^G$ , which describes particles in the GeV energy range. We follow this prescription in calculating the equatorial models, and represent  $K_1$  by linear functions with moderate ( $K_{11}^G = 1 \times 10^{20} \text{ cm}^2 \text{ s}^{-1} \text{ AU}^{-1}$ ,  $K_{11}^A = 0.1 K_{11}^G$ ) and steep ( $K_{11}^G = 5 \times 10^{20} \text{ cm}^2 \text{ s}^{-1} \text{ AU}^{-1}$ ,  $K_{11}^A = 0.1 K_{11}^G$ ) gradients. The values of  $K_{10}^G$  and  $K_{10}^A = 0.1 K_{10}^G$  are chosen in that way that the average value of  $K_1^G$  in the upwind region (i.e. over 100 AU), is in both cases similar and amounts to  $K_1^G \sim 7 \times 10^{22} \text{ cm}^2 \text{ s}^{-1}$ . In the polar wind, the average value must be increased to avoid singularities in the solutions. To simplify the considerations we take the constant value of  $K_1^G = 1 \times 10^{23} \text{ cm}^2 \text{ s}^{-1}$ , which is probably the upper limit of possible coefficients, and tune the value of  $K_1^A$  to obtain the physically meaningful solutions.

All models are summarized in Table 1.

Two other quantities, important in evaluating the obtained solutions, are the pressure of galactic cosmic rays far away from

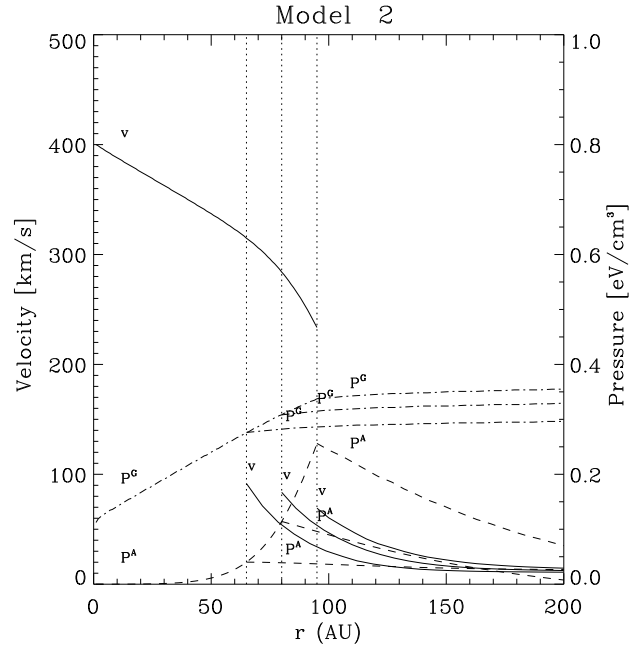


**Fig. 3.** The same plot as in Fig. 2 for model 2. The  $\varepsilon$  values are 0.0, 0.04, and  $\geq 0.15$ .

the Sun ("at infinity") and the pressure of the local interstellar medium. According to Lee & Axford (1988), the LISM pressure should be in the range  $0.5 - 1 \text{ eV cm}^{-3}$ , the upper value being more likely. These values are uncertain mainly due to our very limited knowledge about soft (MeV) galactic cosmic rays in the LISM. In consequence, one can argue for either subsonic or supersonic LISM (Zank et al, 1996b). For the galactic rays pressure, we assume  $P_\infty^G = 0.33 \text{ eV cm}^{-3}$  (Axford, 1985).

We have found that the correct value of the LISM pressure at the heliopause is obtained for only a narrow interval of  $\varepsilon$ , which, however, changes for different  $r_{\text{sh}}$ . Values of  $\varepsilon$  smaller than the lower limit of the mentioned interval result in an increase of the downwind ACR pressure with distance, which corresponds to the source at infinity, not at the shock. The large  $\varepsilon$ , on the other hand, forces a steep negative gradient of the ACR pressure at the shock, which, in consequence, leads to unphysical, negative values of the ACR pressure in the downwind region (Fig. 1).

### 3.1. Equatorial models

The results of four equatorial models are showed in Figs. 2-5. Three quantities: velocity, galactic and anomalous cosmic rays pressure are plotted here as functions of the heliocentric distance for the assumed shock positions at 65, 80, and 95 AU. The presented solutions correspond to the largest possible  $\varepsilon \in (0, 0.15)$  still yielding a non-negative ACR pressure in the downwind region.

*Velocity.* As the result of mass loading the upwind velocity decreases with distance, first linearly, then with an increasing gradient. Clearly, the models 3 and 4, with a smaller pick-up ion production also show a smaller velocity decrease. The steeper

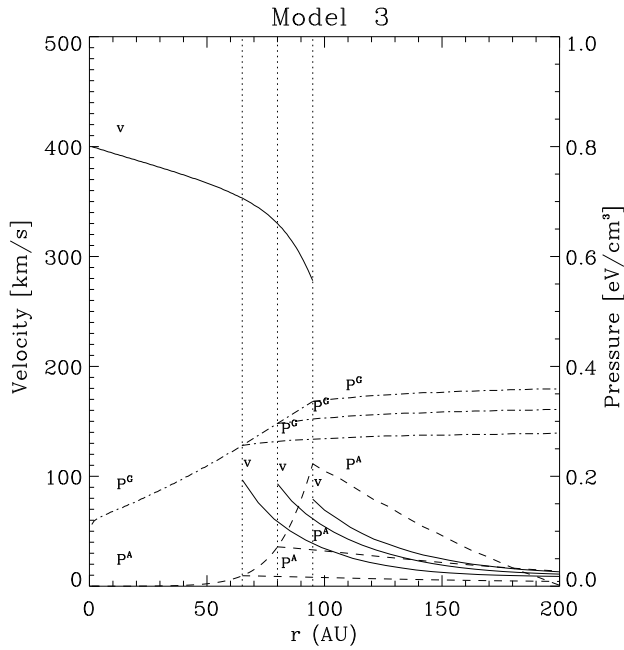


**Fig. 4.** The same plot as in Fig. 2 for model 3. The  $\varepsilon$  values are 0.0, 0.01, and 0.05.

gradient of the diffusion coefficients (models 2 and 4) results in a very efficient slowing down of the flow; velocities at the most distant shock position (95 AU) are quite low, about 200 km/s. The velocity profiles for  $r \geq 75$  AU show a strong precursor structure; in each case one observes a thick region of a large negative velocity gradient, that can be interpreted as a precursor of weak shock. In the inner heliosphere the dominant terms in Eq. (24) determining the velocity profile are: the gas pressure gradient and the momentum exchange with neutrals, while near the shock the cosmic rays pressure and the momentum loss to the neutrals dominate.

*GCR pressure.* The galactic cosmic rays pressure increases monotonically, with a faster rate in the upwind, and more slowly in the downwind region. The obtained GCR pressure is, for all models, in the range  $0.30 - 0.45 \text{ eV cm}^{-3}$ , in good agreement with the canonical value of  $P_{\infty}^G - 0.33 \text{ eV cm}^{-3}$ . The more distant the shock, the larger the GCR pressure at the heliopause (i.e., practically, "at infinity").

*ACR pressure.* The anomalous cosmic rays pressure shows the largest variations among different models. Also, for a given model, the ACR pressure at the shock is very sensitive to the shock position. This follows from a strong dependence of  $P^A$  on the velocity; as was explained earlier,  $v$  varies significantly near the shock. One can say also that the ACR diffusion is most efficient at places where the density of scattering centers (solar wind) varies most, i.e. in a heavily mass loaded wind, close to the shock. The form of  $P^A$  in the downwind region is, to a large extent, determined by  $\varepsilon$ ; this parameter appears in the conservation equation (21) and influences the post-shock value of  $P^A$  - the initial condition for the downwind integration. One can see (Table 1), that the shock at 65 AU allows for a very

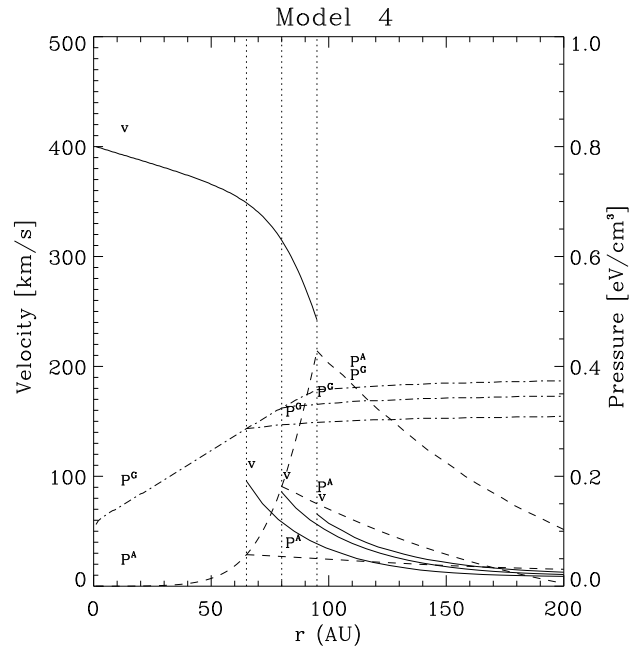


**Fig. 5.** The same plot as in Fig. 2 for model 4. The  $\varepsilon$  values are 0.0, 0.04, and  $\geq 0.15$ .

small  $\varepsilon$  ( $< 0.01$ ) regardless of the model. For  $r_{sh} \sim 80$  AU one gets  $\varepsilon \in (0.01 - 0.09)$ , the upper limit obtained for models with a steep gradient of  $K^A$ . Finally, large  $\varepsilon$  values ( $> 0.15$ ) are still acceptable for the most distant shocks (at 95 AU).

*Gas pressure and magnetic pressure.* Gas pressure dominates the overall pressure near the Sun. It falls down rapidly with the distance, following the density variation. At the shock,  $P$  shows a step-like increase and then decreases slowly towards the heliopause (Fig. 6). This pattern is very similar for all models considered, and the quantitative differences are not large. At the heliopause  $P$  amounts to  $0.05 - 0.35 \text{ eV cm}^{-3}$  and is smaller than  $P^M$ . The magnetic pressure at 200 AU is larger than  $P$  by a factor ranging from 2 ( $r_{sh} = 95$  AU, models 3 and 4) up to 15 ( $r_{sh} = 65$  AU, models 1 and 2). The sum of both pressures, which should balance  $P_{LISM} = 1.0 \text{ eV cm}^{-3}$  at the heliopause, vary between  $0.4 - 1.2 \text{ eV cm}^{-3}$ , depending on the model and  $r_{sh}$ . In general, it decreases with the shock distance and is larger for a smaller pick-up ion production rate. In Fig. 6 we also show a profile of the polytropic pressure variation, that starts from the same value as  $P$  at 1 AU. Even if the difference between the polytropic and nonpolytropic pressure at the shock is somehow exaggerated here (the density profile in the polytropic model would be different from the value of  $\rho$  obtained in our model), one still may come to the conclusion that quantitative results obtained from the polytropic models must be treated with great caution.

*Density.* The source term in Eq. (26) increases the solar wind density above the value that would be obtained for a mass conserving flow. For an efficient mass loading (models 1 and 2) the increase amounts to 10% at 80 AU and 12% at 95 AU. The

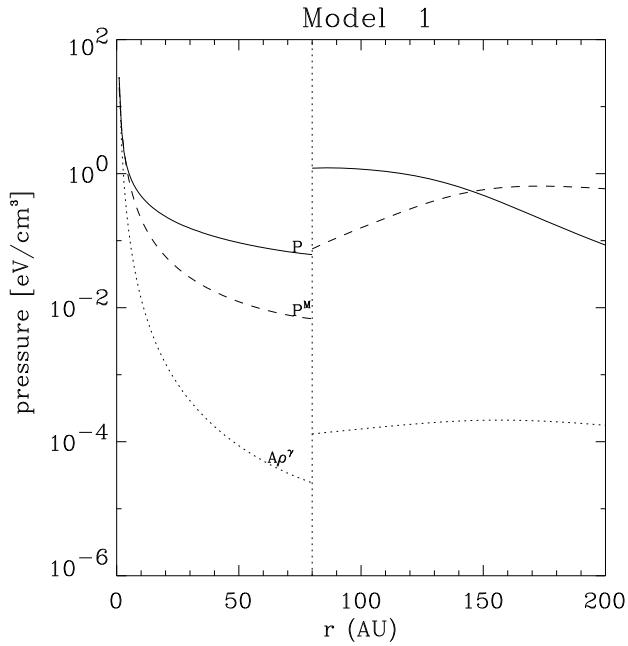


**Fig. 6.** Gas pressure  $P$  and magnetic pressure  $P^M$  as functions of distance for model 1. The shock is set at 80 AU. The polytropic pressure (dotted line) is shown for comparison with  $P$  obtained from a nonpolytropic model.

models with low source-rate of pick-up ions show an increase of about 2-3%.

*Compression ratio.* For a single-fluid, classical shock with  $\gamma = 5/3$  one obtains  $q = 4$ . As mentioned earlier, two opposite effects included in our equations can modify this canonical value: production of ACRs leads to an increase of  $q$ , the mass loading of the wind with pick-up ions results in  $q$  smaller than 4. In Fig. 7 we present the compression ratio as a function of  $r_{\text{sh}}$  obtained for four equatorial models and two values of  $\varepsilon$ : 0.05 and 0.15 (Note, that only for  $r_{\text{sh}} \geq 75$  AU ( $\varepsilon = 0.05$ ) and for  $r_{\text{sh}} \geq 95$  AU ( $\varepsilon = 0.15$ ) some of our models give meaningful solutions for  $P^A$  in the downwind region). For  $\varepsilon \leq 0.1$ , the mass loading effect dominates the ACR production and the resulting  $q$  is smaller than 4. It can be as small as 2.7-2.8 for a distant shock, small  $\varepsilon$  ( $\sim 0.05$ ), and the model with the efficient pick-up ion source.

### 3.2. Polar models

Similarly as for the equatorial models, we consider two different production rates of pick-up ions. The main difference with respect to the equatorial case is a change of the cosmic rays diffusion coefficients. An attempt to use the same values as for the equatorial models was unsuccessful: either the obtained  $P_\infty^G$  was too large, or, what was even worse, the solutions of (26)-(30) appeared to be singular in the upwind region. Therefore, we had to change  $K^G$  and  $K^A$ . An increase of  $K_1^G$  to about  $10^{23}$   $\text{cm}^2 \text{s}^{-1}$  ensures that the obtained  $P_\infty^G$  is approximately correct. In order to avoid singularities in the solution,  $K_1^A$  must be larger

than  $10^{22}$   $\text{cm}^2 \text{s}^{-1}$ . The above numbers correspond to the upper limits of diffusion coefficients considered in the literature. In what follows, we will present the results obtained for a constant  $K_1^G = 10^{23}$   $\text{cm}^2 \text{s}^{-1}$  and  $K_1^A$  varying from  $1.18 \times 10^{22}$   $\text{cm}^2 \text{s}^{-1}$  to  $2. \times 10^{22}$   $\text{cm}^2 \text{s}^{-1}$  (Figs. 8-11). The ACR pressure close to the shock is extremely sensitive to the  $K^A$  value.

Since the expected distance to the heliopause should be larger in the polar than in the equatorial plane (in the direction towards the stagnation point), we will now consider  $r_{\text{sh}}$  in the range 80-120 AU.

From the physical point of view, the two important differences of the polar flow as compared with the equatorial one are: (i) the wind is faster in the upwind region, and (ii) the magnetic pressure in the downwind region vanishes. The magnetic pressure stabilizes the flow; in the equatorial models the upwind solutions are always regular, while the polar models almost always fail before reaching the heliopause: either the velocity becomes negative or the denominator in (27) goes to zero. One could argue that behind the shock the magnetic field is no longer parallel to the shock and, therefore, the magnetic pressure is not negligible there. However, we decided not to introduce the magnetic pressure and follow the downwind solutions as far as possible. At the point where the calculations are terminated, the solar wind and the GCR pressures are practically constant and can be extrapolated to the heliopause in order to be compared with  $P_\infty^G$  and  $P_{\text{LISM}}$ .

*Velocity.* The polar models show a relatively larger decrease of velocity on the way from 1 AU to the shock than the equatorial models, but this effect results from the larger distance to the shock, not the larger velocity gradient. Again, the models with a less efficient pick-up ion source show a smaller velocity decrease. The impressive slowing down of the solar wind at 100-120 AU in models 12 and 14 follows from a very steep ACR pressure gradient.

*GCR pressure.* The galactic cosmic ray pressure shows similar profiles as in the equatorial cases, it is, however, larger at the heliopause ( $0.35 - 0.55$   $\text{eV cm}^{-3}$ ) because more distant shocks provide an extra room for its increase. The value of  $P_\infty^G$  can be easily decreased by a different choice of initial conditions or  $K^G$ .

*ACR pressure.* The anomalous cosmic ray pressure is very sensitive to the diffusion coefficient. Its moderate change, from  $1.50 \times 10^{22}$   $\text{cm}^2 \text{s}^{-1}$  to  $1.22 \times 10^{22}$   $\text{cm}^2 \text{s}^{-1}$ , yields a dramatic increase of the ACR pressure at the shock (approximately a factor of 4). Such an effect has not been observed for equatorial models, but could not be excluded - we have not tried to explore the whole parameter space.

*Gas pressure and density.* The upwind variations of the pressure are similar in form to the equatorial profiles. The magnetic pressure is zero, therefore downstream of the shock only the gas pressure contributes to the pressure balance at the heliopause. Its value at the heliopause (or at the point where calculations are stopped) decreases with the distance of the shock; for shocks at 80-100 AU,  $P$  is equal to  $1.3 - 2.4$   $\text{eV cm}^{-3}$ , which is too large as compared with the expected LISM pressure. From this point of view only the shocks at 110-120 AU are acceptable

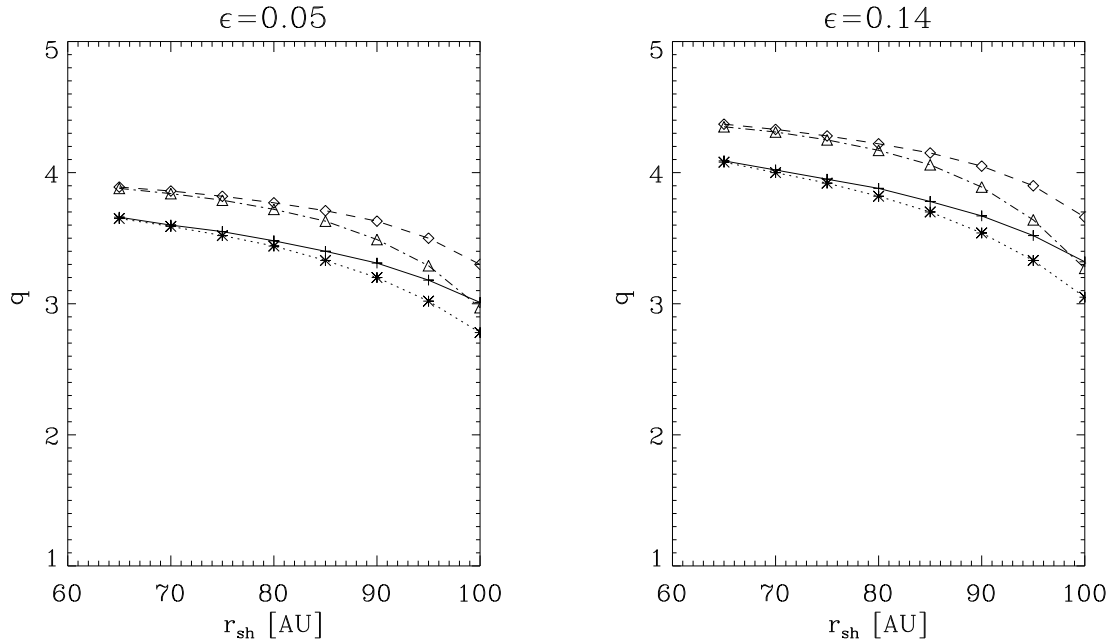


**Fig. 7.** Shock compression ratios  $q$  as functions of the shock distance for the ecliptic solar wind models: 1 (+), 2(\*), 3( $\diamond$ ), 4( $\Delta$ ), and for two values of  $\epsilon$ .

- they yield pressures of  $0.6 - 1.0 \text{ eV cm}^{-3}$ . For models with large anomalous cosmic ray production at the shock (12 and 14), the upstream density shows an interesting feature - it decreases, as one could expect, to a distance of 100 AU but then starts to increase, forming a kind of wall in front of a distant (very weak) shock ( $\sim 120$  AU). This increase is, of course, correlated with a very steep velocity decrease in this region. The mass loading effect amounts to 11-18% at  $r_{\text{sh}} = 80 - 120$  AU for the efficient ionization (models 11, 12), but is 3-4 times smaller for models 13 and 14.

*Compression ratio.* Perhaps the most interesting issue is an appearance of very weak shocks for models 12 and 14. The value of  $q$  can be as small as 1.6-1.8 (Fig. 12). In fact, such structures are very close to a shock-free transition from one flow to another.

#### 4. Summary and conclusions

The model presented in the paper is the first one that simultaneously takes into account three populations of particles: galactic and anomalous cosmic rays as well as pick-up ions, interacting with the magnetized solar wind plasma. The interaction of the solar wind ions with the LISM neutrals is considered in a self-consistent way. When comparing the present model with the classical, two-fluid approach (solar wind + LISM), the main qualitative differences are:

- slowing down of the flow, as the result of additional forces acting in the system (the upwind wind velocity in the outer heliosphere becomes strongly dependent on the heliocentric distance)

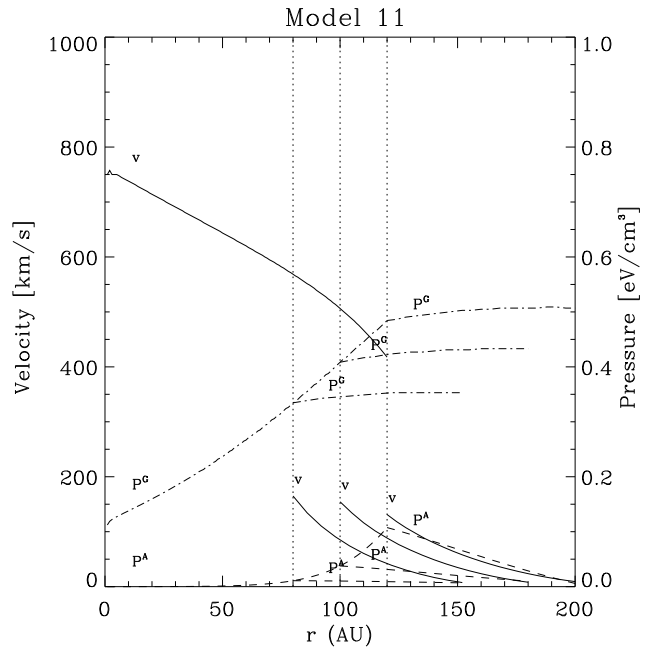


**Fig. 8.** The same plot as in Fig. 2 for model 11. The  $\epsilon$  values are 0.0, 0.01, and 0.04.

- changes in the shock compression ratio. The interaction with LISM neutrals, i.e. the mass loading of the solar wind by the pickup ions, significantly decreases the wind Mach number and the shock becomes weaker; the compression ratio decreases. Taking into account the production of the superthermal population at the shock leads, on the other hand,

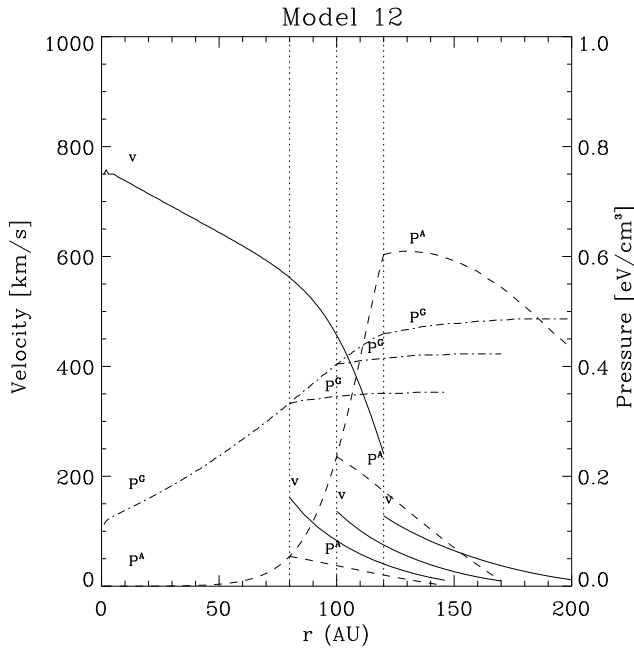


**Fig. 9.** The same plot as in Fig. 2 for model 12. The  $\varepsilon$  values are 0.0, 0.07, and  $\geq 0.15$ .

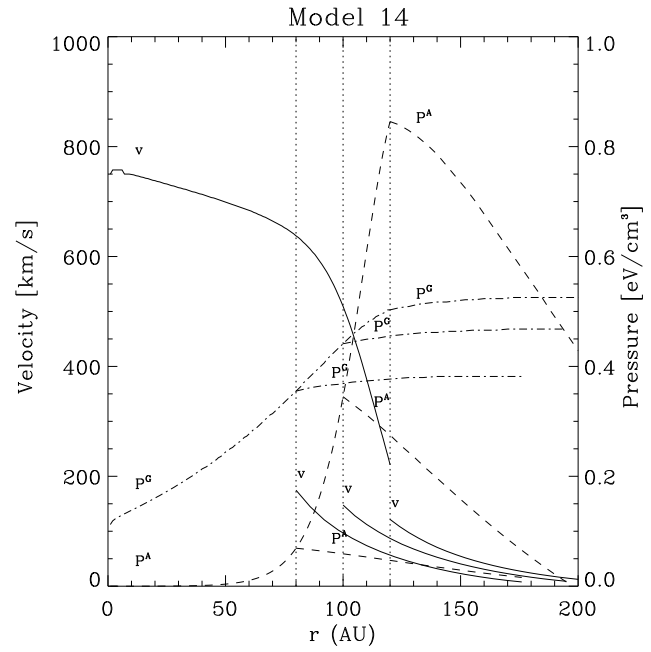


**Fig. 11.** The same plot as in Fig. 2 for model 14. The  $\varepsilon$  values are 0.0, 0.04, and  $\geq 0.15$ .

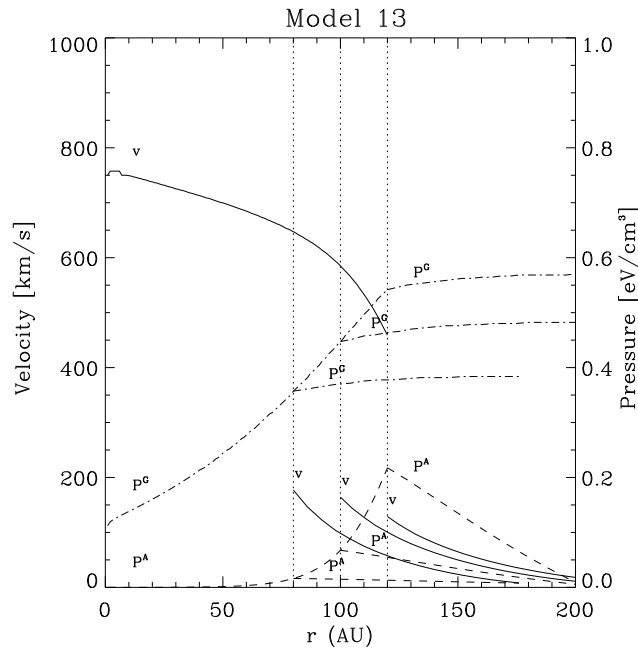


**Fig. 10.** The same plot as in Fig. 2 for model 13. The  $\varepsilon$  values are 0.0, 0.01, and 0.10.

to large compression ratios; the shock generating the superthermal population is stronger than the normal gasdynamical one. The net effect depends on the relative strength of these mechanisms.

- changes in the shock radius. The upwind gradient forces,  $dP/dr$ , as well as the loss of momentum connected with

acceleration of the pickup ions, slow down the upwind flow, which leads to the decrease of  $r_{sh}$ ; the shock moves inward. On the other hand, the sink of the gas energy flux at the shock and the negative gradient of  $P$  lead to the increase of  $r_{sh}$ ; the shock moves outward from the Sun. Because these effects are nonlinear, the net result of these mechanisms is difficult to predict without numerical calculations.

Quantitatively, the above effects can be summarized as follows:

- A. The solar wind termination shock.

The efficiency of ACR production at the shock is in the range 5-10%, if the (ecliptic) shock is at 80-85 AU (i.e. the distance corresponding to the correct values of  $P_{LISM}$  and  $P_{\infty}^G$ ). It can, however, be greater than 15% for distant shocks ( $\geq 120$  AU), with the drawback of a too large  $P_{\infty}^G$  ( $\geq 1.2$  eV/cm<sup>3</sup>). The shock compression ratios lie in the range: 1.6-3.5, i.e. in most cases are much smaller than 4, which means that the mass loading effect prevails over the ACR production. Introduction of ACRs into the model moves the shock out, while the GCRs move it in. The result of the interaction with LISM neutrals is rather to move the shock in. We want to point out that this result is difficult to predict without numerical calculations: one could expect, that the increased upwind pressure will result in the shock being more distant from the Sun, but the decrease in the shock compression ratio is so important, that, in fact, the shock radius is smaller in the presence of pickup ions. Our results agree with the previous findings obtained in simpler approaches (Ko et al. 1988., Ziemkiewicz 1994) that for

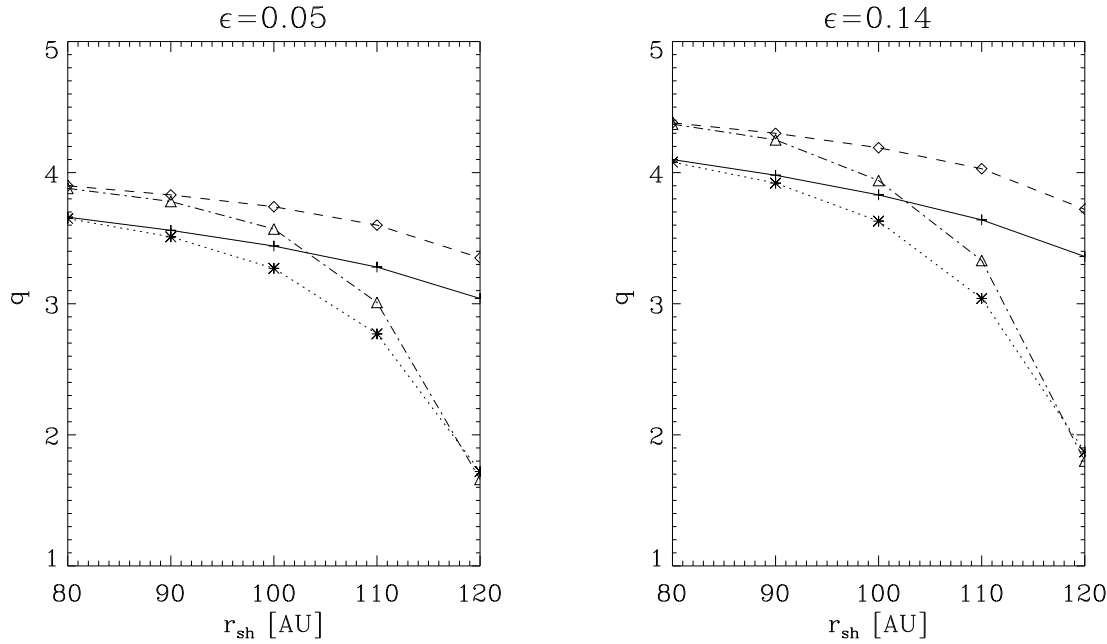


**Fig. 12.** Shock compression ratios  $q$  as functions of the shock distance for the polar solar wind models: 11 (+), 12(\*), 13( $\diamond$ ), 14( $\triangle$ ), and for two values of  $\epsilon$ .

$P_{\infty}^G = 1 \text{ eV/cm}^3$  one obtains  $r_{sh} \sim 80 \text{ AU}$  in the ecliptic plane.

– B The outer heliosphere.

The set of outer heliospheric configurations has been presented for both ecliptic and polar solar winds, showing the spectrum of the possible profiles of the wind velocity and cosmic rays pressure. In the presence of the anomalous component cosmic rays the solar wind is significantly decelerated: to 0.5 – 0.7 of its value at the Earth's orbit, i.e. from 400 km/s at 1 AU to 200-300 km/s at 80 AU (ecliptic plane).

The approximate value of the ACR pressure at the solar wind termination shock is in the range 0.05 – 0.8 eV/cm<sup>3</sup>.

It has already been pointed out several times, that the model presented here is a steady-state one. The heliosphere should, however, be treated as a very unstationary medium; because of the numerous effects, the conditions of the flow are strongly time dependent. Here the problem of the response of the system on the nonlinear, time dependent changes arises; the stationary models are valid only if the relaxation time is short. In the recent literature one can find several models studying the termination shock interactions with different types of time dependent disturbances: from shocks to the very long Alfvén waves (Donohue & Zank 1993, Ziemkiewicz 1995). Donohue & Zank estimated the reformation time after the interaction with an interplanetary shock as about 6 months. With an average termination shock speed of about 100 km/s (Ziemkiewicz, 1995) this corresponds to termination shock oscillations with an amplitude of the order of 10 AU. During the motion of the termination shock its parameters, e.g. the compression ratio, will change. One can consider our steady-state results as corresponding to an average shock radius; on the other hand one can also roughly assess

from them what will be the shock structure at different stages of interaction.

Another apparent disadvantage of our approach is the assumption of spherical symmetry. Therefore, our model describes quite well the upwind region and these parts of the downwind region which are either close to the shock or to the stagnation line. Recently, several groups (e.g. Pauls & Zank, 1996, Zank et al. 1996b) published their multi-dimensional models of the solar wind - LISM interaction, which can reproduce the real shape of the heliopause. These models, however, do not take into account the full interaction with the cosmic rays. Incidentally, their results concerning the termination shock radius are very similar to our values both for the ecliptic and polar cases. For example, the Pauls & Zank's (1996, Table 3) shock radii are 87.5 AU (ecliptic) and 120 AU (polar). In that way, quite surprisingly, our simple approach finds its justification in calculations that are more sophisticated from this point of view.

*Acknowledgements.* The paper was financed from the research project 2 Z6Z6 001 05p13. One of us (J.Z.) was also supported from the project 2 P03C 009 08.

## References

- Axford W.I., 1985, Solar Physics 100, 575
- Axford W.I., Leer E., McKenzie J.F., 1982, A&A 111, 317
- Barnes A. 1993, JGR 98, A4, 15137
- Barnes A. 1994, JGR 99, A4, 6553
- Burton M.E., Smith E.J., Balogh A., et al., 1996, A&A 316, 313
- Chalov S.V., Fahr H.J., 1994, A&A 288, 973
- Chalov S.V., Fahr H.J., 1995, Planet. Sp. Sci 43, No. 8, 1035
- Donohue D.J., Zank G.P., 1993, JGR 98, 19005
- Fahr H.J., Fichtner H., 1991, Sp. Sci. Rev. 58, 193

- Fahr H.J., Ziemkiewicz J., 1988, A&A 202, 295
- Fahr H.J., Grzedzielski S., Ratkiewicz R., 1988, Ann. Geophys. 6, No. 4, 337
- Feldman W.C., Barraclough B.L., Phillips J.L., Wang Y.-M., 1996, A&A 316, 355
- Fichtner H., Fahr H.J., Sreenivasan S.R., 1993, Proc. Int. Conf. Cosmic Rays XXIII 3, 423
- Goldstein B.E., Neugebauer M., Phillips J.L., et al., 1996, A&A 316, 296
- Grzedzielski S., Ziemkiewicz J., 1989, Adv. Sp. Res. 9, No. 4, 239
- Grzedzielski S., Ziemkiewicz J., 1990, in: Proc. 1st COSPAR Coll., eds. E. Page, S. Grzedzielski, p. 363
- Holzer T.E., 1972, JGR 77, 5407
- Isenberg P.A., 1995, Interstellar pickup ions: not just theory anymore, U.S. National Report to Int. Union of Geodesy and Geophysics 1991-1994, p. 623
- Isenberg P.A., Lee M.A., 1995, JGR 100, A9, 17 059
- Jokipii J.R., 1990, Proc. 1st COSPAR Coll., ed E. Page, 169
- Jones F.C., Ellison D.C., 1991, Sp.Sci.Rev. 58, 259
- Ko C.M., 1991, A&A 251, 713
- Ko C.M., Webb G.M., 1987, Ap. J. 323, 657
- Ko C.M., Webb G.M., 1988, Ap. J. 325, 296
- Ko C.M., Jokipii J.R., Webb G.M., 1988, Ap. J. 326, 761
- Ko C.M., Dougherty M.K., McKenzie J.F., 1991, A&A 241, 62
- Lee M.A., 1995, Effects of cosmic rays and interstellar gas on the dynamics of a wind; preprint of the University of New Hampshire
- Lee M.A., Axford W.I., 1988, A&A 194, 297
- McComas D.J., Phillips J.L., Bame B.J., Gosling J.T., Goldstein B.E., Neugebauer M., 1995, Space Sci. Rev. 72, 93
- McKibben R.B., Connell J.J., Lopate C., Simpson J.A., Zhang M., 1996, A&A 316, 547
- Nerney S., Suess S.T., Schmahl E.J., 1991, A&A, 556
- Nerney S., Suess S.T., Schmahl E.J., 1993, JGR 98, 15169
- Pauls H.L., Zank G.P., 1996, JGR 101, 17081
- Potgieter M.S., Le Roux J.A., Burger R.A., 1987, Proc. 20th Cosmic Ray Conf., 3, 287
- Schwenn R., 1990, in: Physics of the Inner Heliosphere, eds. R. Schwenn and E. Marsch, Springer-Verlag, Berlin, p. 99
- Story T.R., Zank G.P., 1995, JGR 100, 9489
- Webb G.M., McKenzie J.F., 1984, J. Plasma Phys. 31, 337
- Webb G.M., Forman M.A., Axford W.I., 1985, Ap. J. 298, 684
- Williams L.L., Zank G.P., Matthaeus W.H., 1995, JGR 100, A9, 17059
- Witte M., Rosenbauer H., Banaszekiewicz M., Fahr H., 1993, Adv. Sp. Res. 93, No. 6, 121
- Zank G.P., 1989, A&A 225, 37
- Zank G.P., Webb G.M., Donohue D.J., 1993, Ap. J. 406, 67
- Zank G.P., Pauls H.L., Cairns I.H., Webb G.M., 1996a, JGR 101, 457
- Zank G.P., Pauls H.L., Williams L.L., Hall D.T., 1996b, JGR 101, 21639
- Ziemkiewicz J., 1994, A&A 292, 677
- Ziemkiewicz J., 1995, JGR 100, A9, 17035
- Ziemkiewicz J., Banaszekiewicz M., 1997, Adv. Sp. Res., 19, No.6, 961